water

MDPI

Article

Research on Geothermal Geology and Heat-Forming Conditions in the Tangyuan Fault Depression

Chang Li [1,2], Shuren Hao [3,*], Chuansheng Li [4,*], Sihong Zhu [4], Lin Guo [1,2], Chen Hu [1,2], Qifa Sun [1,2], Xiuhai Li [5] and Wei Hu [5]

[1] Harbin Center for Integrated Natural Resources Survey, China Geological Survey, Harbin 150086, China; 13845114316@163.com (C.L.)
[2] Observation and Research Station of Earth Critical Zone in Black Soil, Harbin, Ministry of Natural Resources, Harbin 150086, China
[3] School of Civil and Architectural Engineering, East China University of Technology, Nanchang 330013, China
[4] Shandong GEO-Surveying & Mapping Institute, Ji'nan 250012, China; jnzhusihong@163.com
[5] Institute of Ecological Geology Survey and Research of Heilongjiang Province, Harbin 150030, China
* Correspondence: dr_haosr@163.com (S.H.); lichuansheng1983@163.com (C.L.)

Abstract: In order to gain an in-depth understanding of the geothermal geological characteristics and heat-forming conditions in the Tangyuan fault-depression area, this paper has carried out a series of detailed geological works, including geological surveys and geophysical explorations. Through these works, combined with the results of systematic drilling, sampling tests, and dynamic monitoring, we have studied, analyzed, and compared the relevant data to achieve a comprehensive understanding of the geological characteristics in the Tangyuan fault-depression area. During the research process, we preliminarily determined the stratigraphic structure and geological structure in this area and clarified the characteristics of the main geothermal reservoir and its burial conditions. These findings provide basic data support for our understanding of the formation and distribution of geothermal resources. At the same time, we have carried out a systematic analysis of the basic geothermal geological parameters, laying the foundation for the future calculation and evaluation of geothermal resource reserves. Through the collation and analysis of these research results, this paper not only provides a scientific basis for the development of geothermal resources in the Tangyuan fault-depression area but also provides specific references for future development prospect plans. This series of work will lay a solid foundation for further development and utilization of geothermal resources and promote the sustainable development of the regional economy.

Keywords: Yishu graben; geothermal geology; heat-forming conditions; renewable energy

check for updates

Citation: Li, C.; Hao, S.; Li, C.; Zhu, S.; Guo, L.; Hu, C.; Sun, Q.; Li, X.; Hu, W. Research on Geothermal Geology and Heat-Forming Conditions in the Tangyuan Fault Depression. *Water* **2024**, *16*, 2972. https://doi.org/10.3390/w16202972

Academic Editors: Xudong Zhang, Yiding Bao, Xudong Zhou, Shengyi Cong and Shuang Tian

Received: 24 September 2024
Revised: 12 October 2024
Accepted: 14 October 2024
Published: 18 October 2024

Copyright: © 2024 by the authors. Licensee MDPI, Basel, Switzerland. This article is an open access article distributed under the terms and conditions of the Creative Commons Attribution (CC BY) license (https://creativecommons.org/licenses/by/4.0/).

1. Introduction

The importance of researching geothermal genesis mechanisms stems from the potential of geothermal resources as a clean and renewable energy source [1]. The development of geothermal energy not only helps meet the growing energy demands of humanity and reduce dependence on fossil fuels but also contributes to minimizing greenhouse gas emissions and mitigating global climate change [2]. Research on geothermal genesis mechanisms involves multiple disciplines, including geology, geophysics, and geochemistry, which are crucial for understanding the formation, distribution, and utilization of geothermal resources [3]. Early geothermal studies focused on surface phenomena such as hot springs and geysers [4], relying primarily on empirical observations. In the mid-20th century, with advancements in Earth sciences and exploration technologies, the study of geothermal genesis mechanisms gradually deepened. Classical theories include crustal thickness, geothermal gradients, and heat flow migration [5–7]. In recent decades, research has shifted towards utilizing geological structures [8], magma activity [9], and other quantitative methods to explore more complex geothermal systems.

Recent advancements in geothermal research have significantly enhanced our understanding of the distribution and formation mechanisms of geothermal resources. Researchers are focusing on identifying and mapping these resources, particularly in geologically active regions such as tectonic plate boundaries, volcanic arcs, and rift zones. Utilizing advanced geospatial technologies and geophysical methods such as seismic imaging, scientists are creating detailed maps that inform energy policy and development [10].

In addition to distribution, there is a strong emphasis on understanding the mechanisms behind geothermal resource formation. The tectonic control theory and magma activity driving theory highlight the roles of tectonic processes and magma intrusions in generating heat for geothermal systems. For instance, in Japan, geothermal systems are closely associated with volcanic activity, notably in areas such as the Hakone and Kusatsu regions [11]. Similarly, the geothermal fields in New Zealand, such as the Wairakei and Rotokawa, are linked to active geothermal systems resulting from subduction zone processes [12]. Case studies in the United States have shown how mantle hotspots, such as those in Yellowstone National Park, contribute significantly to geothermal activity in stable plate interiors [13]. Other notable examples include the East African Rift, where tectonic activity has led to significant geothermal resource potential [14], and the Andes region, which showcases how volcanic arcs can create substantial geothermal reservoirs [15]. By employing a multi-disciplinary and multi-scale approach, researchers are gaining deeper insights into geothermal systems, which is crucial for sustainable energy development [16,17].

Research on geothermal resources in China started relatively late but has developed rapidly. As early as the 1970s, the Chinese Academy of Geological Sciences began geothermal exploration and research in the Tibetan Plateau and the North China Seismic Zone, achieving a series of significant results [18]. Entering the 21st century, research institutions such as the China University of Geosciences and the Chinese Academy of Sciences conducted detailed studies on geothermal resources in regions such as the North China Plain [19], the Yishu Rift [20], and the Sichuan Basin [21], focusing on the impact of geological structures on geothermal formation. In terms of research methods, domestic scholars adopted comprehensive approaches involving geological exploration technologies, geophysical methods, and geochemical analyses to reveal the characteristics of geothermal systems under different geological backgrounds. In particular, through field geological surveys, drilling, and heat flow measurements, they have deeply explored the geothermal genesis mechanisms in regions such as the North China Block and Jianghan Plain [22].

Currently, research on the Tangyuan Sag primarily focuses on oil and gas reservoirs, tectonic evolution, and sedimentary characteristics [23,24]. These topics dominate the academic discussions in this region, with numerous studies exploring the hydrocarbon potential and revealing important insights into its structural features and sedimentation patterns. However, only Liu Yu has conducted a preliminary evaluation of the geothermal potential in the Tangyuan Sag, noting the existence of geothermal resources; this assessment, however, is relatively superficial and does not explore the underlying mechanisms of geothermal resource formation in depth [25]. As a result, the scientific community's understanding of the unique geological conditions and geothermal characteristics of the Tangyuan Sag remains insufficient, which may limit the comprehensive development of the local geothermal potential.

Given the lack of comprehensive studies on the geothermal genesis mechanisms in the Tangyuan Sag, there is a significant opportunity for further exploration. It is imperative to conduct in-depth research on the geological settings of the area and the thermal dynamics influencing geothermal resource formation. For example, studies conducted in regions such as the Yellow River fault and the Penglai area in China have shown that tectonic movements and sedimentary environments play a crucial role in the formation of geothermal resources. Research on the Yellow River fault area has demonstrated that volcanic activity and fault movements work together to create significant geothermal flow [26]. Meanwhile, studies in the Penglai area reveal the influence of fracture systems on the movement of geothermal fluids [27].

By drawing on these cases, our research aims to fill the existing gap in understanding the geothermal genesis mechanisms in the Tangyuan Sag. We will employ advanced methodologies such as geophysical logging and controlled-source audio-frequency magnetotellurics to analyze the geological and geochemical characteristics of the Tangyuan Sag, thereby delving into the factors that influence the formation of geothermal resources [28]. Ultimately, this research aims to provide a more comprehensive understanding of the geothermal potential in the Tangyuan Sag and to contribute valuable insights for sustainable resource development in the region.

2. General Situation of the Research Area

The Tangyuan fault depression represents a first-order tectonic unit located at the northernmost end of the Tan-Lu fault system. This geographical feature spans the regions of Hegang City, Tangyuan County, Luobei County, and Huachuan County in Heilongjiang Province, encompassing an area of approximately 3320 square kilometers, with a width ranging from 5 to 20 km as shown in Figure 1. The boundaries of this fault depression are primarily controlled by two deep-seated, large-scale faults that extend roughly parallel in a northeast (NE) direction, resulting in a long, narrow fault-depression basin aligned with this orientation.

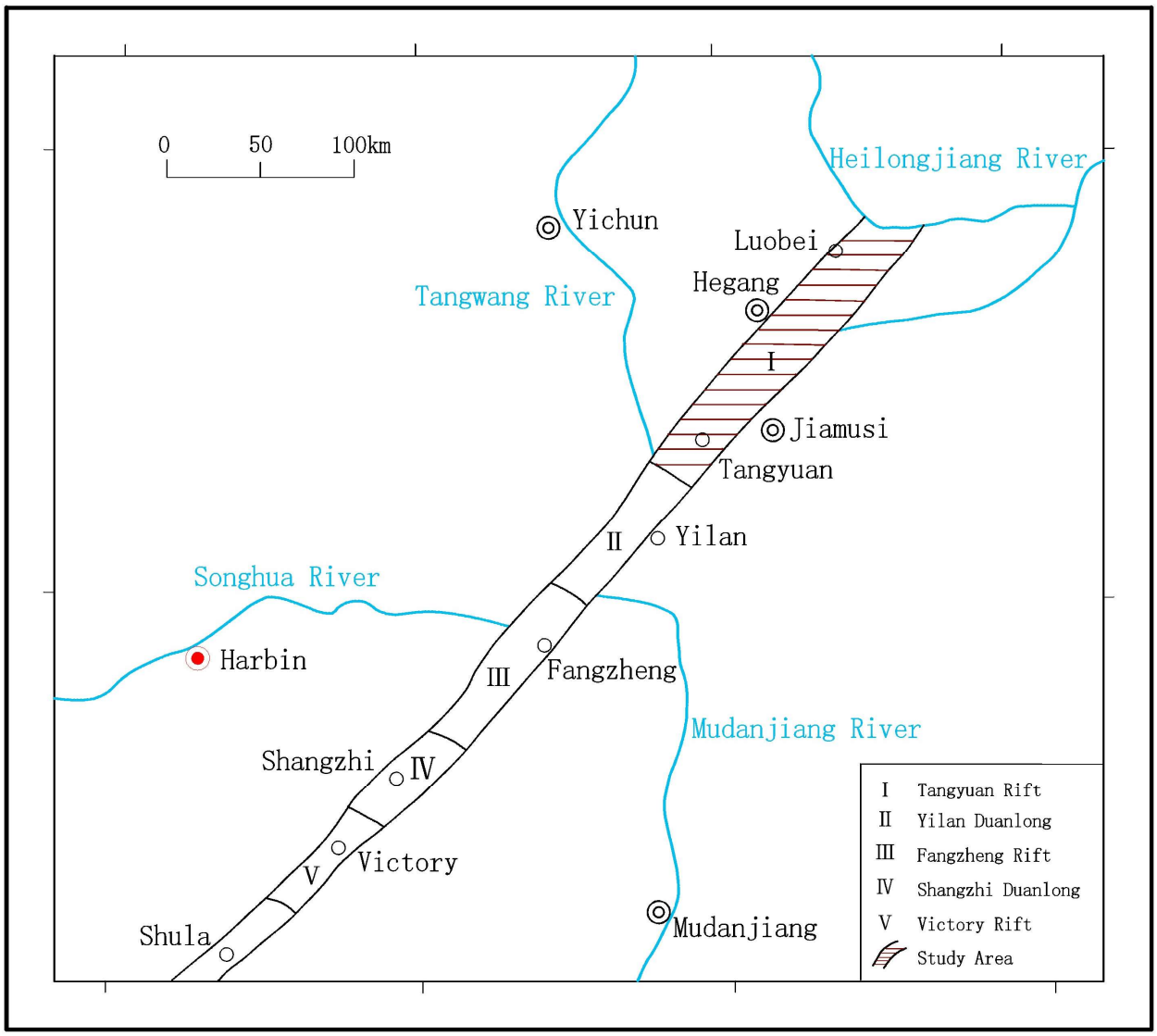

Figure 1. Location map of the study area.

Tectonically, the research area is situated within the Hegang Uplift, which is part of the second uplift zone of the Neocathaysian tectonic system. The southeastern portion of the area falls within the Sanjiang subsidence zone, also within this second uplift zone. The graben is characterized by the deposition of thick Paleogene strata. Throughout the Mesozoic era, volcanic activity and migmatization processes were relatively prevalent within the graben, contributing to the development of faults of varying grades and characteristics.

The research area lies at the intersection of the northernmost segment of the Yishu Graben and the Sanjiang Plain, positioned on the Paleozoic uplift zone of the Bureya-Jiamusi block, as illustrated in Figure 1. According to the tectonic classification of Heilongjiang Province, this area is categorized under the Laoyeling block (V) within the Khanka–Bureya Mountain block, specifically within the Sanjiang new fault-depression zone (V4) and the Mingshan fault depression (V41).

The geothermal fields within the research area are significantly influenced by the underlying graben structures. The distribution of the Tangyuan fault depression defines the extent of the geothermal field, which covers approximately 66.6 square kilometers. The boundaries of this geothermal field in a southeast–northwest (SE-NW) orientation are chiefly regulated by two waterproof boundaries that extend parallel with a strike of NE45°. Overall, this area is characterized as a strip-shaped, graben-like fault-depression basin, with a width of 6–8 km and an extension in the NE45° direction. The basement lithology of the geothermal fields consists primarily of extensive Hercynian and Yanshanian granites, while the sedimentary strata are predominantly Paleogene in origin, featuring a total thickness of approximately 3000 m.

The sedimentary layers overlying the Paleozoic metamorphic basement in this fault depression primarily consist of Paleogene and Quaternary strata. Notably, the Baoquanling Formation of the Paleogene serves as the main target layer for the exploration of underground hot water resources within the research area, exhibiting a sedimentary thickness ranging from 500 to 2500 m. Below, the characteristics of each formation section are briefly described according to the stratigraphic sequence as shown in Table 1:

In the Tangyuan fault-depression zone, magmatic activities are notably intense, large-scale, and frequent, primarily concentrated within the fault zone and the extensive areas on either side. These magmatic activities, which are associated with the gestation, formation, and evolution of the boundary faults in this zone, primarily began during the Mesozoic era, with significant activity noted particularly in the Yanshanian period.

(1) Temporal and Spatial Characteristics of Mesozoic Magmatic Activities

In the early Mesozoic era, following the collision between the Siberian plate and the North China plate, the entire region experienced uplift, leading to the formation of continental structures and the establishment of the Eurasian continental plate. This was followed by successive interactions between the Eurasian plate and both the Izanagi and Pacific plates, which resulted in the development of a series of northeast (NE) or north-northeast (NNE)-trending fold and fault-depression belts across Northeast China. Within this geological context, varying intensities and scales of magmatic activities occurred in the Yishu fault zone and its surrounding areas during the Mesozoic period. Volcanic eruptions during the Yanshanian period predominantly produced andesite, rhyolite, and andesitic pyroclastic rocks, all of which belong to the cal-alkaline series.

(2) Temporal and Spatial Characteristics of Cenozoic Magmatic Activities

Cenozoic magmatic activities are primarily characterized by fissure-type to central-type overflow activities involving basic magma. These activities are predominantly situated at the intersections of the Yishu fault zone with northwest (NW)-trending or nearly east–west (EW)-trending faults.

Table 1. Regional stratigraphic table.

Stratigraphic Age (Code)				Thickness (m)	Main Lithology
Series	**System**	**Formation**	**Code**		
Quaternary System	Holocene Series		Qh	3–10	The lithology is silty clay and fine silt sand, and the lower part is yellow-brown sandy gravel.
	Upper Pleistocene Series	Belahonghe Formation	Q3pb	5–30	It is composed of yellow-brown silty clay, gray-black muddy silty clay, and yellow-brown and off-white sandy gravel and gravel.
	Middle Pleistocene Series	Nongjiang Formation	Qpn	30–40	Gray sandy gravel and pebble gravel.
	Lower Pleistocene Series	Suibin Formation	QpS	40–50	Medium-coarse sand, sandy gravel, and gravel.
Neogene System	Middle-Pliocene Series	Fujin Formation	Nf	360	The lithology is off-white and gray-green medium-fine sandstone and medium-coarse sandstone.
Paleogene System	Eocene-Oligocene Series	Baoquanling Formation	Eb	2500	Gray, off-white, and gray-green glutenite, sandstone, and silty mudstone are in interbeds with unequal thicknesses and contain coal.
Cretaceous System	Upper Series	Songmuhe Formation	K2s	>1190	It is composed of intermediate-acid, intermediate-basic and acid lava as well as their tuff and tuff lava.

3. Geothermal Geology Research Area Plan

3.1. Geophysical Well Logging

Well Luo-re 1 is sited 200 m south of Yufeng Village in Zhaoxing Town, with a designed depth of 1870 m. Geophysical logging of Well Luo-re 1 was conducted using the SDZ-3000 logging tool (Zonge International, Tucson, AZ, USA), undertaken twice. The first logging session occurred between 0 and 400 m before casing was installed, following the completion of the first drilling phase. The second logging session spanned from 400 to 1870 m, also conducted prior to casing installation after the second drilling phase. The logged parameters included resistivity, spontaneous potential, acoustic slowness, natural gamma radiation, well temperature, caliper measurements, hole deviation, shale content, effective porosity, permeability, and water saturation. These logging results were instrumental in accurately identifying the geothermal reservoir aquifer sections.

3.2. Controlled-Source Audio-Frequency Magnetotelluric Sounding

The layout of survey lines for this geophysical exploration is based on the principle of delineating the boundaries of the Yishu Graben and identifying sections within the graben where geothermal resources are best preserved. The survey lines are oriented perpendicular to the strike of the graben.

The Controlled-Source Audio-Frequency Magnetotelluric (CSAMT) method is an electromagnetic sounding technique that employs a finite-length grounded dipole as the field source. Simultaneous observations of electrical and magnetic field parameters are taken at specified distances from the dipole center. In this research, an equatorial dipole device is utilized for scalar measurements. Specifically, the horizontal component of the electric field (Ex), parallel to the field source, and the horizontal component of the magnetic field (Hy), orthogonal to the field source, are recorded (refer to Figure 2 for the layout of the equatorial dipole measurement device in the CSAMT method).

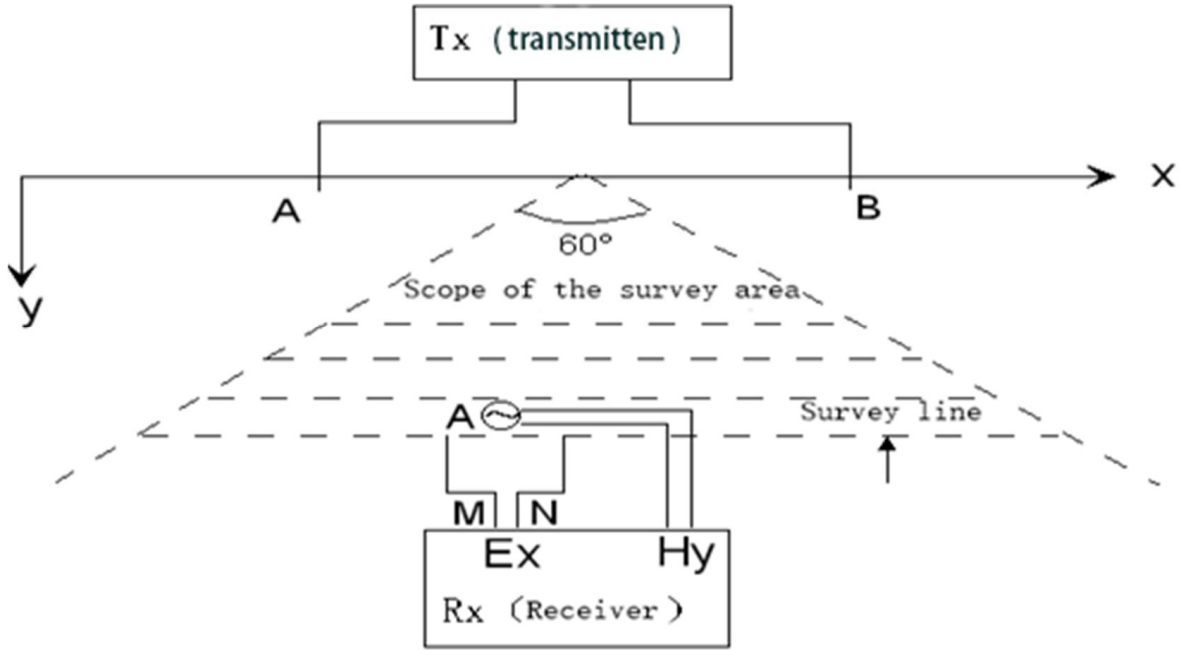

Figure 2. Schematic diagram of the measurement device for the controlled-source electromagnetic sounding method.

The impedance resistivity ρs is calculated using the amplitudes of the electric field *Ex* and the magnetic field *Hy*, while the impedance phase φs is derived from the phases *Ep* and *Hp* of the electric and magnetic fields, respectively. Both the impedance resistivity and impedance phase are subjected to joint inversion to determine the resistivity parameters related to Controlled-Source Electromagnetic Sounding. Geological interpretations and inferences are subsequently conducted based on the results of this inversion.

For the fieldwork associated with the Controlled-Source Audio-Frequency Magnetotelluric Sounding, the GDP-32 multifunction electrical method instrument (China Electronics Technology Group Corporation 22th Research Institute (CETC 22), Xinxiang, He'nan, China) was employed, functioning within a frequency range of 0.125 Hz to 8192 Hz. A total of three survey lines were established in a northwest–southeast direction, featuring a line spacing of 3.5 km and a cumulative survey line length of 32 km as shown in Figure 3.

Survey Line Details:

Line 1: This line measured 14 km in total length, with 8.5 km situated within the survey area. The point spacing was set at 50 m, resulting in a total of 280 measurement points, 170 of which were located within the survey area.

Line 2: With a total length of 10 km, this line extended 5.5 km within the survey area. It also utilized a point spacing of 50 m, yielding 200 measurement points, of which 110 were within the designated survey area.

Line 3: This line, measuring 8 km in length, was positioned between Lines 1 and 2. The point spacing for Line 3 was 100 m, resulting in 80 measurement points.

This work completed a total of 560 coordinate points, with 360 points surveyed within the investigation area and 19 quality check points, accounting for 3.39% of the total measurement points. The average relative mean square error of apparent resistivity is 1.90%. The quality of the above work meets the corresponding specifications, and the collected data can be used for further processing and interpretation. Statistical errors for quality checks are shown in Table 2.

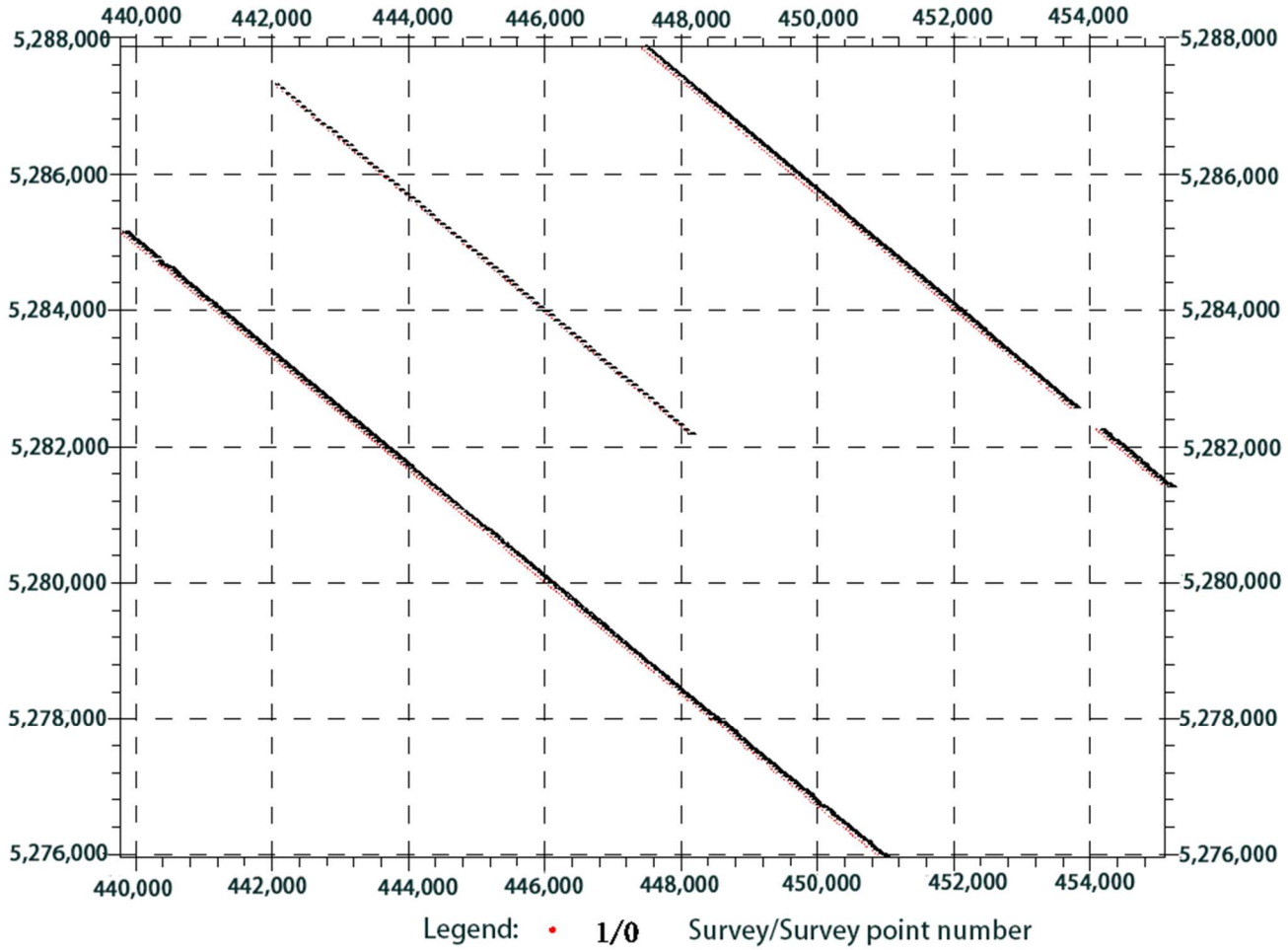

Figure 3. Location map of survey points.

Table 2. Statistical Table of Quality Check Errors for Controlled Source Audio-Frequency Magnetotelluric Survey.

Serial Number	Point/Line Number	Error
1	−5400/1	2.95%
2	−5350/1	1.90%
3	−5300/1	1.89%
4	−5250/1	2.65%
5	−5200/1	1.43%
6	−5150/1	1.11%
7	7800/1	0.93%
8	7950/1	2.16%
9	8000/1	1.57%
10	8050/1	1.64%
11	7200/2	1.09%
12	7250/2	0.68%
13	7300/2	0.85%
14	7350/2	0.85%
15	7400/2	0.80%
16	1500/3	4.89%
17	1700/3	3.49%
18	4100/3	2.05%
19	4600/3	3.11%
Overall average mean square error of apparent resistivity: 1.90%.		

Through the inversion of the collected data, depths of over 3000 m were achieved, and an inversion resistivity cross-section diagram was created. Based on the resistivity profiles derived from the CSAMT inversion, geological interpretations were conducted to infer the distribution of faults within the measured profiles. Predictions regarding geothermal resources along the profiles were made, leading to the recommendation of two well locations for future geothermal development. All design and specification requirements were effectively met. Figure 2 illustrates the location map of the Controlled-Source Audio-Frequency Magnetotelluric Sounding measurement points in the area, with the survey lines laid out in the 130° direction.

4. Detection Results and Analysis of Geothermal Reservoir Characteristics

4.1. Analysis of Geophysical Well-Logging Results

4.1.1. Stratigraphy

Through a comprehensive analysis of the construction of Well Luo-re 1, combined with geophysical well logging and various logging methods, the stratigraphic situation in the research area has been delineated. The stratigraphic sequence revealed by the borehole, from top to bottom, is as follows:

Quaternary Strata: Comprising loess-like silty clay, loose gravel, and sand-mud, with a burial depth of 0–100 m.

Neogene Fujin Formation: Characterized by off-white and gray-green medium-fine sandstone and medium-coarse sandstone, with a burial depth of 110–360 m.

Paleogene Eocene-Oligocene Baoquanling Formation: This formation exhibits a diverse lithology including off-white sandstone, variegated glutenite, gray siltstone, mudstone, and oil shale in its upper section. Local intercalated coal seams containing resin are present, along with thick mudstone layers in the lower section. The Baoquanling Formation has a burial depth ranging from 360 to 1780 m and has yet to be fully drilled through.

4.1.2. Characteristics of Geothermal Reservoirs

The type of geothermal field in the research area is categorized as medium-low temperature (II) type II-1, representing an exploratory type of layered geothermal reservoir. The geothermal reservoirs are distributed within the Paleogene sandstone layers located inside the Tangyuan fault depression, and their overall shape is approximately parallelogrammatic.

The cap rock of the geothermal reservoir consists of a thick mudstone layer from the Baoquanling Formation, exhibiting average waterproof and heat-insulation properties. The geothermal reservoir layer is characterized by the sandstone found in the Baoquanling Formation. This sandstone is primarily off-white and gray, featuring argillaceous cementation, poor diagenesis, and relatively loose grains. The main components include quartz, feldspar, and a small proportion of dark minerals, predominantly concentrated at depths of 899 to 1400 m (see Table 3). From top to bottom, there is a gradual strengthening of cementation and diagenesis, a change in grain size from coarse to fine, an increase in argillaceous content, and a decrease in porosity.

Table 3. Statistical Table of the Thermal Reservoir in Well LuoRe 1.

Layer Number	Well Interval	Thickness	Argillaceous Content	Porosity	Permeability	Water Saturation	Formation Temperature
	m	m	%	%	10^{-3} μm^2	%	°C
1	899.3–900.9	1.6	26.4	25.4	149.2	100.0	37.5
2	903.4–905.6	2.2	21.7	27.0	200.0	100.0	37.6
3	906.6–909.6	3.0	31.1	22.1	94.3	100.0	37.7
4	917.3–920.9	3.6	25.0	24.8	135.4	100.0	38.0
5	922.4–923.9	1.5	24.9	24.8	132.3	100.0	38.0
6	933.0–936.8	3.8	36.0	19.3	53.3	100.0	38.3
7	941.6–947.4	5.8	22.8	25.9	168.5	100.0	38.6
8	963.6–965.1	1.5	34.1	17.4	30.5	100.0	39.0

Table 3. *Cont.*

Layer Number	Well Interval	Thickness	Argillaceous Content	Porosity	Permeability	Water Saturation	Formation Temperature
	m	m	%	%	10^{-3} μm^2	%	°C
9	967.6–973.0	5.4	23.1	23.4	114.0	100.0	39.1
10	983.8–992.9	9.1	19.9	26.6	172.6	100.0	39.5
11	995.3–1007.9	12.6	22.2	25.1	142.7	100.0	39.8
12	1013.1–1020.0	6.9	35.1	20.0	63.8	100.0	40.3
13	1022.1–1028.6	6.5	35.6	19.7	50.4	100.0	40.6
14	1030.4–1039.9	9.5	38.5	18.0	40.4	100.0	40.8
15	1040.6–1045.1	4.5	29.8	20.8	75.1	100.0	41.0
16	1059.8–1100.1	40.3	31.1	19.1	45.2	100.0	42.3
17	1211.4–1223.0	11.6	28.1	19.8	59.6	100.0	46.5
18	1224.6–1226.0	1.4	38.8	15.7	18.1	100.0	46.6
19	1227.3–1230.3	3.0	25.1	20.9	64.4	100.0	46.7
20	1231.0–1234.6	3.6	40.9	15.0	19.9	100.0	46.8
21	1236.0–1239.1	3.1	36.7	15.8	24.6	100.0	46.9
22	1251.6–1255.8	4.2	30.3	17.9	35.4	100.0	47.2
23	1256.5–1262.9	6.4	29.0	18.8	46.6	100.0	47.3
24	1263.9–1265.9	2.0	27.7	18.9	48.1	100.0	47.4
25	1267.0–1268.4	1.4	34.8	14.5	17.1	100.0	47.5
26	1271.1–1273.1	2.0	24.4	20.9	59.2	100.0	47.5
27	1339.1–1347.1	8.0	24.8	18.9	62.3	100.0	49.1
28	1350.3–1351.3	1.0	31.2	15.8	17.3	100.0	49.2
29	1354.1–1355.5	1.4	41.8	12.6	8.7	100.0	49.3
30	1359.1–1360.5	1.4	39.6	13.9	13.1	100.0	49.7
31	1363.8–1368.4	4.6	30.7	16.6	46.1	100.0	49.9
32	1371.5–1377.4	5.9	24.0	20.3	70.6	100.0	50.2
33	1380.6–1386.1	5.5	32.9	15.9	19.9	100.0	50.4
34	1388.5–1393.1	4.6	28.9	17.3	36.4	100.0	50.5
35	1412.0–1418.1	6.1	22.8	17.1	28.5	100.0	50.9
36	1420.3–1425.1	4.8	17.9	20.7	61.0	100.0	51.2
37	1426.6–1431.3	4.7	35.3	14.8	13.3	100.0	51.4
38	1435.9–1439.6	3.7	36.0	15.3	17.1	100.0	51.5
39	1444.0–1447.4	3.4	32.2	16.2	24.5	100.0	51.7
40	1461.5–1464.8	3.3	25.3	17.6	29.1	100.0	52.3
41	1466.8–1468.4	1.6	40.5	11.7	4.9	100.0	52.5
42	1470.1–1472.0	1.9	26.1	16.2	24.3	100.0	52.6
43	1503.4–1505.1	1.7	40.4	11.3	5.7	100.0	53.4
44	1517.8–1521.5	3.7	21.7	16.6	27.8	100.0	53.8
45	1526.6–1528.8	2.2	24.6	18.4	33.0	100.0	53.8
46	1538.6–1542.3	3.7	37.0	13.2	9.2	100.0	54.0
47	1543.1–1544.3	1.2	32.4	13.4	8.1	100.0	54.1
48	1546.1–1551.8	5.7	32.1	13.7	10.7	100.0	54.2
49	1552.8–1553.6	0.8	31.1	12.7	8.4	100.0	54.3
50	1574.5–1580.3	5.8	25.9	12.9	11.0	100.0	54.9
51	1582.1–1588.8	6.7	29.7	13.0	10.6	100.0	55.3
52	1594.3–1595.9	1.6	26.6	15.0	22.3	100.0	55.6
53	1599.6–1602.9	3.3	22.9	12.1	6.7	100.0	55.7
54	1607.1–1616.8	9.7	16.4	15.6	17.5	100.0	56.1
55	1627.5–1629.0	1.5	36.1	10.6	3.1	100.0	56.4
56	1630.1–1637.3	7.2	26.6	13.7	12.7	100.0	56.6
57	1639.1–1641.5	2.4	26.0	13.7	11.0	100.0	56.7
58	1642.1–1643.9	1.8	29.8	11.8	4.9	100.0	56.8
59	1646.8–1648.6	1.8	35.2	10.2	2.7	100.0	56.9
60	1649.6–1653.4	3.8	22.4	14.7	13.7	100.0	57.0
61	1654.3–1656.5	2.2	30.7	11.9	5.1	100.0	57.0
62	1659.9–1663.4	3.5	27.0	12.6	7.7	100.0	57.2
63	1664.3–1670.5	6.2	28.6	10.5	3.7	100.0	57.3
64	1672.4–1675.5	3.1	17.2	11.7	7.0	100.0	57.4
65	1689.0–1696.4	7.4	29.5	8.6	2.2	100.0	57.4
66	1696.8–1701.3	4.5	25.0	9.8	3.4	100.0	57.5
67	1701.9–1708.5	6.6	25.7	8.2	1.5	100.0	57.6
68	1747.5–1749.4	1.9	25.8	11.6	6.8	100.0	58.8

1. The geothermal reservoir layers with a permeability greater than 100 (10^{-3} μm²) are mainly distributed at a depth of 899–1000 m. There are 8 layers, with an average shale content of 23.3%, an average porosity of 25.2%, a maximum single-layer thickness of 12.6 m,

a minimum single-layer thickness of 1.5 m, an average single-layer thickness of 5.2 m, a total thickness of 41.8 m, and an average geothermal reservoir temperature of 38.5 °C.

2. The geothermal reservoir layers with a permeability of 30–100 (10^{-3} μm²) are mainly concentrated at a depth of 1000–1400 m and are divided into two types of geothermal reservoir layers according to the permeability.

(1) There are 11 geothermal reservoir layers with a permeability of 50–100 (10^{-3} μm²). The average shale content is 28.4%, the average porosity is 20.3%, the maximum single-layer thickness is 11.6 m, the minimum single-layer thickness is 2.0 m, the average single-layer thickness is 5.45 m, the total thickness is 60 m, and the average temperature of the geothermal reservoir is 44.5 °C.

(2) There are 9 geothermal reservoir layers with a permeability of 30–50 (10^{-3} μm²). The average shale content is 30.5%, the average porosity is 18.0%, the maximum single-layer thickness is 40.3 m, the minimum single-layer thickness is 1.5 m, the average single-layer thickness is 8.4 m, the total thickness is 75.3 m, and the average temperature of the geothermal reservoir is 46.5 °C.

3. There are 40 geothermal reservoir layers with a permeability less than 30 (10^{-3} μm²). The average shale content is 30.4%, the average porosity is 13.4%, the maximum single-layer thickness is 9.7 m, the minimum single-layer thickness is 0.8 m, the average single-layer thickness is 3.3 m, the total thickness is 141.3 m, the average temperature of the geothermal reservoir is 53.8 °C, and they are mainly distributed below 1400 m.

In total, there are 68 identified water-bearing layers, with a cumulative thickness of 318.4 m. The water-bearing layers associated with the geothermal reservoir are primarily concentrated in the upper sections, gradually becoming less favorable downward. In accordance with geological exploration regulations for geothermal resources, water-bearing layers with a permeability greater than 50 (10^{-3} μm²) are classified as geothermal reservoir layers. Integrating the well-logging temperature data reveals that Well Luo-re 1 contains 19 geothermal reservoir layers, with a total thickness of 101.8 m.

4.1.3. Characteristics of the Geothermal Field

The geothermal temperature recorded at a depth of 1000 m in Well Luo-re 1 is 40.1 °C, while at a depth of 1800 m, the temperature reaches 60.1 °C. This indicates that the geothermal gradient in the research area is approximately 2.5 °C per 100 m.

In the Quaternary and Neogene strata, the temperature remains relatively stable, indicating proximity to the constant-temperature layer. Below 500 m, the geothermal temperature curve for the Baoquanling Formation exhibits a mostly linear relationship, indicating consistent temperature changes. The geothermal gradient is slightly elevated in the mudstone sections, whereas it is comparatively lower in the sandstone sections.

4.2. Analysis of CSAMT Results

Figure 4 is the inversion resistivity cross-section diagram of Line 1 in the area. It can be seen from the figure that the inversion resistivity curve is basically of the KHA type. In the shallow part of the cross-section, there is relatively high resistivity, and after passing through the high-resistivity area, there is relatively low resistivity. After reaching a certain depth, the resistivity gradually increases as the depth increases. There are obvious lateral resistivity mutation zones near—2700 m and 2900 m respectively. It is inferred that these lateral resistivity mutation zones are caused by fault structures (numbered as F3 and F4 respectively).

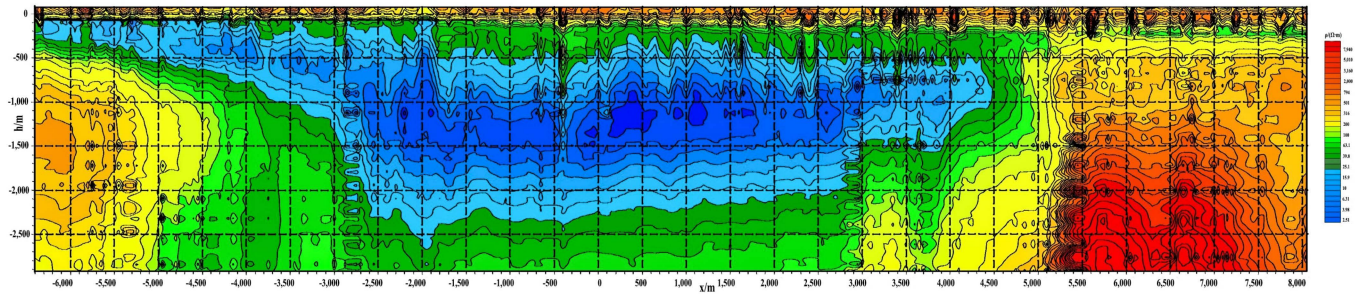

Figure 4. CSAMT inverted resistivity section diagram of survey Line 1.

Figure 5 is the geological interpretation cross-section diagram of Line 1. According to the inferred inversion resistivity, the thickness of the high-resistivity layer on the surface is about 100 m, and the thickness of the low-resistivity layer below the high-resistivity layer varies greatly. F3 and F4 are the main faults controlling the fault-depression basin in the profile. According to the inferred inversion resistivity, the fault displacement of F3 exceeds 1000 m. The low-resistivity layer in the central part of the basin is very thick, and the maximum thickness of the low-resistivity layer at less than 10 Ω·m exceeds 700 m, and the maximum depth of the basement burial exceeds 2500 m.

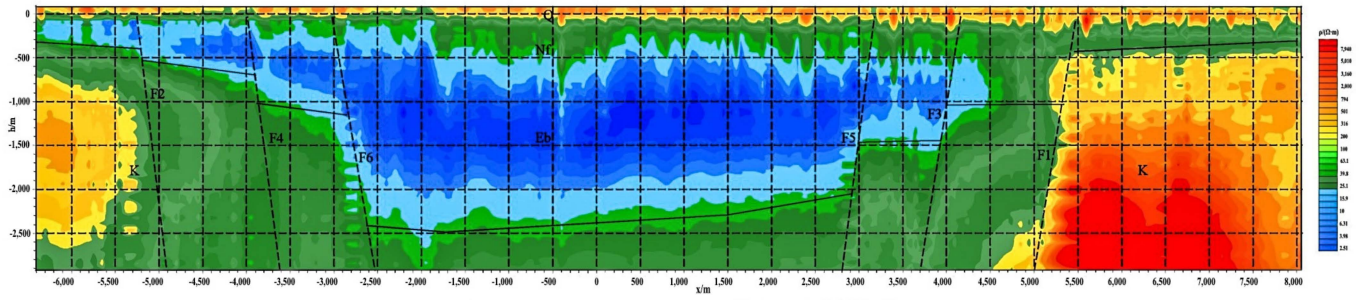

Figure 5. CSAMT geological interpretation section diagram of survey Line 1.

Figure 6 is the inversion resistivity cross-section diagram of Line 2 in the area. As can be seen from the figure, similar to Line 1, the inversion resistivity curve of Line 2 is basically of the KHA type. In the shallow part of the cross-section, there is relatively high resistivity, and after passing through the high-resistivity area, there is relatively low resistivity. After reaching a certain depth, the resistivity gradually increases as the depth increases.

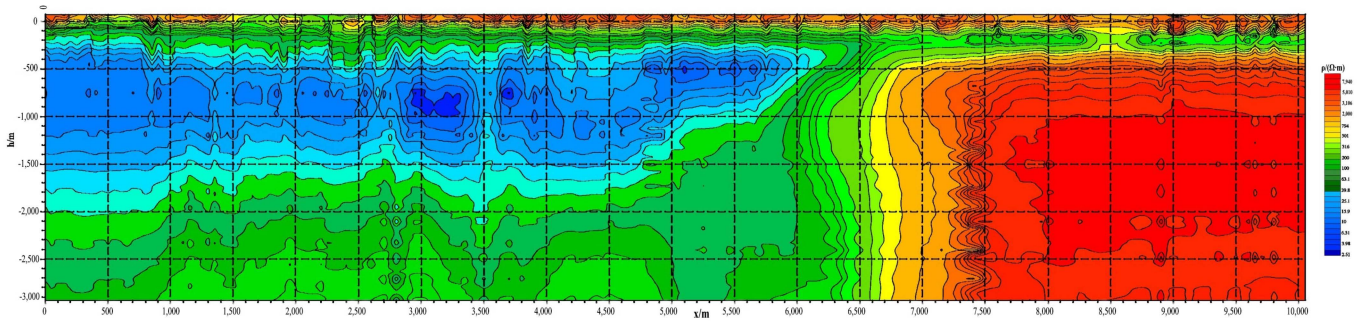

Figure 6. CSAMT inverted resistivity section diagram of survey Line 2.

A weak lateral resistivity mutation zone appears near x = 5000 m. It is inferred that these lateral resistivity mutation zones are caused by fault structures (numbered as F4).

Figure 7 is the geological interpretation cross-section diagram of Line 2. It can be seen from the figure that the profile does not pass through the northwest section of the fault-depression basin. The thickness of the high-resistivity layer on the surface of the section is

more than 100 m, and the thickness of the low-resistivity layer below the high-resistivity layer varies greatly. The maximum thickness of the low-resistivity layer at less than 10 Ω·m is more than 700 m. Similarly, F4 is the main fault controlling the southeast side of the fault-depression basin in the profile. According to the inferred inversion resistivity, the maximum burial depth of the basement in the section passed by the Line 2 profile is more than 2100 m.

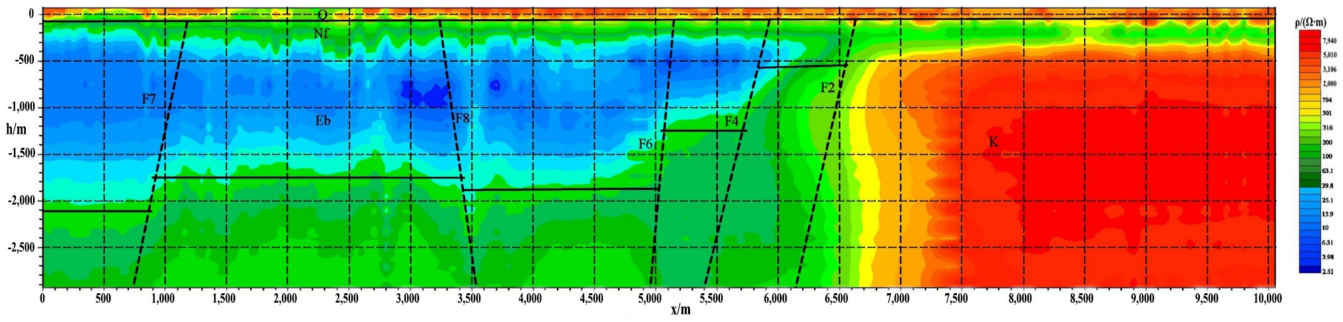

Figure 7. CSAMT geological interpretation section diagram of survey Line 2.

Figure 8 is the geological interpretation cross-section diagram of Line 3. According to the resistivity differences in the contact areas of the three blocks, two faults are identified. And compared with the already surveyed L1 and L2 lines, it is found that the three profiles are in very good agreement. The fault at point 600 is Fault F1, and the fault at point 3000 is Fault F3. Although the point spacing of Line L3 is larger than that of Lines L1 and L2, reaching 100 m, and the details are not as well depicted as Lines L1 and L2, the overall area division is relatively clear and can be mutually verified with other lines, achieving the purpose of the work.

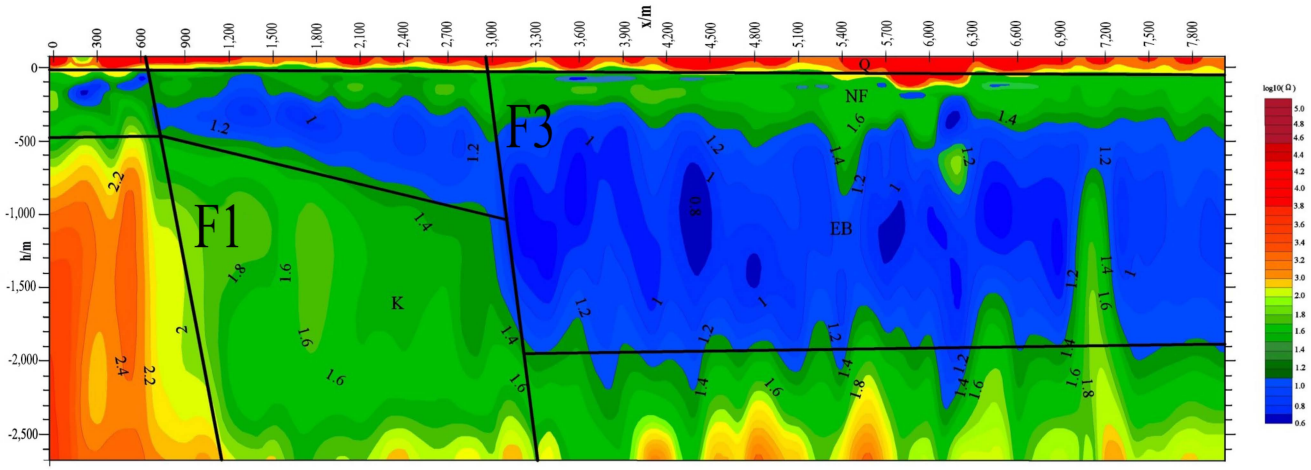

Figure 8. CSAMT geological interpretation section diagram of survey Line 3.

5. Discussion

5.1. Analysis of Geothermal Genesis Mechanisms

The burial conditions of geothermal resources are closely related to multiple factors, including cap rock, geothermal reservoirs, heat sources, and the recharge of geothermal water in geothermal fields. Based on the results of geophysical exploration, exploration Line 1 (see Figure 5) crosses the entire graben, exploration Line 2 (see Figure 7) traverses the southern boundary of the graben, and exploration Line 3 (see Figure 8) spans its northern boundary. By integrating these three exploration lines, drilling data, and previous geological information, it can be preliminarily inferred that the width of the graben is about 6 to 8 km and is controlled by multiple parallel faults. This observation is similar to

other geothermal projects in China, such as those in Sichuan and Yunnan, where geological features reflect the close relationship between the formation of geothermal resources and their structural environment [29,30].

5.1.1. Geothermal Reservoir Cap Rock

The geothermal resources in this region are primarily of the low-temperature hot water type, characterized by deep burial and heat conduction. The cap rock of the geothermal reservoir is formed by a combination of Quaternary loose sediments, Neogene strata, and the upper part of the Paleogene strata, with a total thickness of approximately 900 m. The lithology consists of silty clay, unconsolidated gravel-sand layers, unconsolidated sandstone layers, and mudstone layers. These cap rocks, with their low density and poor thermal conductivity, serve as effective insulating layers that prevent heat loss. Compared to some regions with volcanic rock cap layers, such as those in Yunnan, this area has an ideal thickness but may exhibit lower thermal conductivity [31].

5.1.2. Geothermal Reservoir

In the study area, the geothermal reservoir is primarily located in the middle and lower sections of the Baoquanling Formation. This formation consists of fine-grained sandstone, medium-grained sandstone, medium-coarse-grained sandstone, argillaceous sandstone, and sandy mudstone, where the loose bonding between particles allows for high porosity, thereby creating an excellent heat storage space. The lithology and pore structure of geothermal reservoirs are critical for their thermal storage capacity and developability. Based on the electrical resistivity inversion results, the surface high-resistivity layer is approximately 100 m thick, while the thickness of the low-resistivity layer varies significantly, with key faults F1 and F2 further influencing the distribution of geothermal resources. This contrasts with the scenarios observed in other developed regions, confirming the impact of structural features on geothermal resources [32].

5.1.3. Heat Source

The heat sources in this study area are primarily derived from normal heat conduction within the deep crust. During the expansion of the graben, particularly in the Paleogene sedimentary period, the formation of multiple faults played an important role in the transmission and exchange of deep heat sources. This is consistent with the experiences of other geothermal-active regions globally, such as in Japan and Italy, where heat sources are similarly influenced by tectonic movements. Additionally, the gravitational compressive heat generated by the thick Neogene sedimentary layers within the sedimentary basin further enriches the heat sources in this area. The chemical reactions releasing heat from widespread coal-bearing strata in the Paleogene also contribute to the regional heat supply, enhancing the diversity of heat sources available [33,34].

5.1.4. The Recharge Sources of Geothermal Water

In the study area, apart from water retained during sediment deposition and sedimentary water, the majority of the underground hot water is recharged laterally through sedimentary layers over prolonged periods. This recharge pathway has also been recognized as a significant mechanism for geothermal water generation in the Sichuan and Yunnan regions. Overall, the formation of underground hot water is primarily due to atmospheric precipitation gathering to form surface runoff, which subsequently undergoes vertical infiltration. This mechanism aligns closely with other regions, although variations may arise due to differing geological conditions and precipitation levels. Moreover, driven by hydraulic head differences, the flowing water heats up and undergoes water-salt reactions within the rock layers, resulting in shifts in the quality of the geothermal water.

5.2. Development Prospect and Economic Benefit Analysis

5.2.1. Development Prospects

The development prospects for geothermal resources in this region are promising, primarily due to the favorable geological conditions observed in the Baoquanling Formation. With geothermal reservoirs located at depths ranging from 900 to 2000 m, the potential for extracting low-temperature hot water is significant. This situation not only allows for effective utilization in residential heating and industrial applications but also offers opportunities for district heating systems and greenhouse agriculture. Successful case studies from other regions in China, such as those in Sichuan and Yunnan, demonstrate that well-managed geothermal projects can yield substantial returns and contribute to local economic growth. As the demand for renewable energy sources continues to rise, the strategic development of geothermal resources can position this region as a leader in sustainable energy solutions, aligning with national goals for green energy and reduced carbon emissions.

5.2.2. Economic Analysis

In line with the "Geological Exploration Standards for Geothermal Resources" (GB11615-2010) [35], the economic feasibility of exploiting geothermal resources in this area can be classified based on well depth. Wells less than 1000 m deep are considered the most economical due to their low development costs, allowing for rapid returns on investment. The primary geothermal reservoirs in this area, located at depths below 2000 m, fall into the "economical" category. While the initial investment for drilling may be higher than for shallow wells, the potential for stable economic returns remains strong through effective management and operational practices. Together with the successful experiences from regions such as Sichuan and Yunnan, the economic landscape for geothermal development in this region appears favorable, promoting both investment and sustainability in energy resources [30,31].

6. Conclusions

(1) Geological conditions in the research area

The landform of the research area is an alluvial low plain, with an altitude ranging from 60 to 70 m. Generally, the terrain slopes from southwest to northeast. It is located at the confluence of the northernmost end of the Yishu Graben and the Sanjiang Plain. It is situated on the Paleozoic uplift zone of the Bureya-Jiamusi massif. According to the tectonic division of Heilongjiang Province, it belongs to the Laoyeling massif (V) in the Khanka-Bureya massif area, the Sanjiang new fault-depression zone (V_4), and the Mingshan fault depression (V_4^1). The scope and distribution of geothermal fields in the research area are controlled by the graben structure in the area. Generally, it is a graben-type fault-depression basin in a strip shape, which is 6–8 km wide and extends in the NE-45° direction. The stratigraphic sequence in the research area is as follows: The lithology of the Quaternary strata is loess-like silty clay, loose gravel-sand, and sand-mud, with a burial depth of 0–100 m; the lithology of the Neogene Fujin Formation strata is off-white and gray-green medium-fine sandstone and medium-coarse sandstone, with a burial depth of 110–360 m; the lithology of the Paleogene Eocene-Oligocene Baoquanling Formation strata is off-white sandstone, variegated glutenite, gray siltstone, mudstone, and oil shale in the upper part, with local coal seams containing resin in the coal seams, and thick-layer mudstone in the lower part, with a burial depth of 360–3000 m.

(2) Geothermal reservoir conditions in the research area

The research area belongs to the low-temperature type II–1 layered geothermal reservoir. The cap rock of the geothermal resources is mainly the mudstone of the Baoquanling Formation above 900 m. The geothermal reservoir layer is mainly the loose sandstone layer of the Paleogene Baoquanling Formation with a burial depth of 900–1400 m. The cumulative thickness of the geothermal reservoir layer is 101.8 m (calculated according to the geothermal reservoir layer with a permeability greater than 50×10^{-3} μm²). The geothermal

reservoir temperature is 39–60 °C, which belongs to the warm-water to warm-hot-water level.

(3) Promising prospects for geothermal development

The geothermal resources in the Baoquanling Formation offer strong development potential due to favorable geological conditions and depths suitable for economical exploitation. With reservoirs between 900 and 2000 m deep and insights from successful projects in Sichuan and Yunnan, the region is poised to effectively utilize geothermal energy for heating and sustainability. Despite higher initial investments, the prospects for stable returns align with national renewable energy goals, fostering local economic growth and environmental sustainability.

Author Contributions: Conceptualization, C.L. (Chang Li); Methodology, C.L. (Chuansheng Li) and L.G.; Software (winglink 2.10.1), W.H.; Validation, L.G.; Formal analysis, C.H. and X.L.; Investigation, C.L. (Chuansheng Li); Resources, S.Z.; Data curation, S.H. and C.H.; Writing—original draft, S.H.; Writing—review & editing, S.H. and W.H.; Visualization, Q.S. and X.L.; Project administration, S.Z. and Q.S.; Funding acquisition, C.L. (Chang Li). All authors have read and agreed to the published version of the manuscript.

Funding: This research was funded by China Geological Survey: DD20230470.

Data Availability Statement: Data are contained within the article.

Conflicts of Interest: The authors declare no conflict of interest.

References

1. He, P. Hydrogeochemistry and Genesis of Low Temperature Geothermal Systems in the Southeast Margin of Guangdong Nankun Hills, Guangdong Province. *Guangdong Chem. Ind.* **2024**, *51*, 130–133.
2. Chen, Q.; Wang, X. Geothermal energy: Moving towards the center of the world energy stage. *China Petroleum News*, 22 September 2023; p. 2.
3. Du, J.; Wang, Z.; Li, F.; Xu, Z.; Zhu, X.; Wang, R.; Xu, Z. Discussion on the development and utilization mode of geothermal resources. *Pop. Stand.* **2023**, *19*, 83–85.
4. Liu, Y. A Study of Hydrochemistry and Geyser of Thermal Groundwater in the Banglazhang Geothermal Field in Longling, Yunnan. Ph.D. Thesis, China University of Geosciences, Beijing, China, 2009.
5. Bai, F. Characteristics of geothermal field in northern Shaanxi and comprehensive development and utilization of oil, gas and geothermal energy. In Proceedings of the 2022 International Conference on Oil and Gas Field Exploration and Development I, Xinjiang, China, 16–18 August 2022; Research Institute of Shaanxi Yanchang Petroleum (Group) Co., Ltd.: Xi'an, China, 2022.
6. Gui, K.; Han, J.; Shi, M. Measurement of Heat and Mass Transport Properties of Porous Mesia with the Constant Heat Flux. *Acta Metrol. Sin.* **1995**, *4*, 252–256.
7. Popov, Y.A.; Pribnow, D.F.; Sass, J.H.; Williams, C.F.; Burkhardt, H. Characterization of rock thermal conductivity by high-resolution optical scanning. *Geothermics* **1999**, *28*, 253–276. [CrossRef]
8. Xie, Y.; Zheng, H.; Liang, Y.; Duo, J.; Song, R.; Wang, Y.; Zheng, F.; Chen, H. Geothermal geological conditions and resource formation factors in the South China Sea Basin. *J. Chengdu Univ. Technol. (Nat. Sci. Ed.)* **2023**, *50*, 647–660.
9. Hu, T. Exploring Magmatism in the Harmonious Metabolism of the Earth:An Endless Source of Geothermal Energy. *Coal Geol. China* **2024**, *36*, 38–41.
10. Han, J.; Niu, P.; Liu, L. Research Status and Prospect of Deep Driving Mechanism of Co-Occurrence of Geothermal Resources and Seismic Activity. *J. Jilin Univ. (Earth Sci. Ed.)* **2023**, *53*, 1950–1968.
11. Aghahosseini, A.; Breyer, C. From hot rock to useful energy: A global estimate of enhanced geothermal systems potential. *Appl. Energy* **2020**, *279*, 115769. [CrossRef]
12. Sandra, M.; Narayanamoorthy, S.; Suvitha, K.; Pamucar, D.; Simic, V.; Kang, D. An insightful multicriteria model for the selection of drilling technique for heat extraction from geothermal reservoirs using a fuzzy-rough approach. *Inf. Sci.* **2025**, *686*, 121353. [CrossRef]
13. Duan, W.; Shi, L.; Luo, C.F.; Li, S.; Li, D. Response of clastic reservoir to magmatic intrusion: Advances and prospects. *Geoenergy Sci. Eng.* **2023**, *227*, 211938. [CrossRef]
14. Suzuki, H.; Kasahara, K.; Ohtake, M.; Takahashi, A.; Ikawa, T.; Abe, S.; Kawabe, Y. Underground structure and magmatic activity of Izu-Oshima volcano, Japan as inferred from seismic reflection survey. *J. Volcanol. Geotherm. Res.* **1992**, *49*, 105–117. [CrossRef]
15. Montaggioni, L.F.; Pons-Branchu, E.; Fournier, F.; Martin-Garin, B.; Dapoigny, A.; Marié, L.; Salvat, B. Revisiting the geodynamical history of the so-called uplifted atolls, north-west Tuamotu, French Polynesia, central South Pacific. *Earth-Sci. Rev.* **2023**, *244*, 104532. [CrossRef]

16. Devine, J.D.; Sigurdsson, H. Petrology and eruption styles of Kick'em-Jenny submarine volcano, Lesser Antilles island arc. *J. Volcanol. Geotherm. Res.* **1995**, *69*, 35–58. [CrossRef]
17. Devine, J.D.; Sigurdsson, H. The liquid composition and crystallization history of the 1979 soufriere magma, St. Vincent, W.I. *J. Volcanol. Geotherm. Res.* **1983**, *16*, 1–31. [CrossRef]
18. Du, J. Geological conditions of gold deposits in xiaotian Mesozoic volcanic basin, Anhui Province. *Precious Met. Geol.* **1992**, *4*, 207–213.
19. Chang, E. The Relationship between geotemperature field and deep-seated structure in the north of north china plain. *Compr. Brig. Chin. Acad. Geol. Sci.* **1989**, *562*, 281–294.
20. Wang, S. The Geothermal Favorable Area Prediction for Fangzheng Fault Depression in Yi-shu Graben. Ph.D. Thesis, Jilin University, Changchun, China, 2018.
21. Sun, D.; Li, J.; Cao, N.; Li, Z.; Zhang, Z.; Xie, X.; Yuan, M.; Cai, H. A preliminary study of the geothermal geological characteristics and exploration potential of the Sichuan Basin. *Hydrogeol. Eng. Geol.* **2023**, *50*, 193–206.
22. Chen, M.; Wang, J.; Wang, J.; Deng, X.; Yang, S.; Xiong, L.; Zhang, J. Geothermal characteristics and genetic mechanism in North China. *Acta Geol. Sin.* **1990**, *1*, 80–91.
23. Cui, C. Simulation of Pool-Forming History of Paleogene in Tangyuan Fault Depression. Ph.D. Thesis, Northeast Petroleum University, Daqing, China, 2017.
24. Wang, H.; Yang, J.; Lin, D. Combination of paleogene sandstone heavy mineral and source analysis in Tangyuan Rift. *Pet. Geol. Oilfield Dev. Daqing* **2007**, *3*, 39–42+46.
25. Liu, Y. Evaluation of geothermal resources in Tangyuan fault Depression, Yishu Fault zone, Heilongjiang Province. *Sci. Technol. Innov. Appl.* **2014**, *7*, 109.
26. Qi, Y.; Wang, Y.; Yao, L. Geological structure of the lower reaches of the Yellow River (Henan Section) the influence of geothermal distribution analysis. *J. North China Water Conserv. Hydropower Univ. (Nat. Sci. Ed.)* **2020**, *9*, 67–72. [CrossRef]
27. Zuo, T.; Li, X.; Wang, J.; Hu, Q.; Tao, Z.; Hu, T. Insights into natural tuff as a building material: Effects of natural joints on fracture fractal characteristics and energy evolution of rocks under impact load. *Eng. Fail. Anal.* **2024**, *163*, 108584. [CrossRef]
28. Xiao, T.; Huang, X.; Cheng, L.; Song, T.; Wang, G.; Yang, B.; Wang, Y. The Effects of Magnetic Susceptibility on Controlled-Source Audio-Frequency Magnetotellurics. *Pure Appl. Geophys.* **2022**, *179*, 2327–2349.
29. Zhang, H.; Chen, Y.; Wang, M.; Song, Y. Thermal evolution differences of reservoir bitumen and their implications: A case study of the Moxi area in the central Sichuan basin. *Mar. Pet. Geol.* **2024**, *169*, 107039. [CrossRef]
30. Li, J.; Zhang, X.; Xu, C.; Li, C.; Tan, H.; Yu, Z.; Zhang, Y. Evaluation of Medium-Deep Geothermal Resources Based on Seismic Imaging Technology: A Case Study of the Midu Basin in Yunnan Province. *Energies* **2024**, *17*, 3948. [CrossRef]
31. Zhang, L.X.; Liu, Z.H.; Chen, K. Geothermal Geology Characteristic and Origin Analysis of Shilin Basin in Yunnan Province. *Adv. Mater. Res.* **2013**, *2592*, 1449–1452. [CrossRef]
32. Zi, F.; Xiao, W.; Sami, M.; Zhang, C.; Xie, F.; Liu, Y.; Li, S. Understanding the genesis of ore-bearing and ore-barren adakitic rocks: Insights from geochronology and geochemical analysis of the Tuncang intrusion and enclaves along the South Tan-Lu Fault. *Int. J. Earth Sci.* **2024**, 1–20. [CrossRef]
33. Guowen, W.; Jian, K. Genetic Analysis of Geothermal Resources in Deep-Seated Fault Area in Tonghe County, Northeast China and Implications of Geothermal Exploration. *Sustainability* **2022**, *14*, 5431. [CrossRef]
34. Zhang, X.; Ye, P.; Wu, Y.; Zhai, E. Experimental study on simultaneous heat-water-salt migration of bare soil subjected to evaporation. *J. Hydrol.* **2022**, *609*, 127710. [CrossRef]
35. *GB11615-2010*; Geologic Exploration Standard of Geothermal Resources. China Standards Press: Beijing, China, 2011.

Disclaimer/Publisher's Note: The statements, opinions and data contained in all publications are solely those of the individual author(s) and contributor(s) and not of MDPI and/or the editor(s). MDPI and/or the editor(s) disclaim responsibility for any injury to people or property resulting from any ideas, methods, instructions or products referred to in the content.